Theory of magnetic textures in high-T_c superconductors: electron versus hole doping dependence

1995 J. Phys.: Condens. Matter 7 1335

(http://iopscience.iop.org/0953-8984/7/7/015)

J. Phys.: Condens. Matter 7 (1995) 1335–1349. Printed in the UK

Theory of magnetic textures in high-T_c superconductors: electron versus hole doping dependence

Weiyi Zhang† and K H Bennemann‡

† National Laboratory of Solid State Microstructures and Department of Physics, Nanjing University, 210008 Nanjing, China

‡ Institute for Theoretical Physics, Freie Universität Berlin, Arnimallee 14, D-14195 Berlin, Germany

Received 19 September 1994, in final form 29 November 1994

Abstract. Various magnetic textures in the CuO_2 planes of high-T_c superconductors are studied using the three-band Hubbard Hamiltonian. In particular, the electron and hole doping dependence is determined. The textures studied for a lattice of supercells consisting of 4×4 CuO_2 cells include an antiferromagnetic state (AF), a spiral-like state, a vortex-like state, as well as domain structures. The relative stability of the magnetic textures is determined by using the unrestricted Hartree–Fock approximation and the real space recursion method. At the critical doping concentration for the destruction of the AF state, we find that domain-like textures have the lowest energy for hole doping and the spiral- and domain-like textures have the lowest energy for electron doping. In general, we obtain that the doping effect is intrinsically asymmetrical for electron and hole doping: the antiferromagnetic state is less rapidly destroyed in the case of electron doping, in agreement with experimental results.

1. Introduction

For high-T_c superconducting oxides, both hole- and electron-doped systems have been studied experimentally. In the case of hole-doped oxides, such as $La_{2-x}Sr_xCuO_4$ [1] and $YBa_2Cu_3O_{7-\delta}$ [2], the conducting carriers have a hole-like character. In the electron-doped oxides, such as $Nd_{2-x}Ce_xCuO_{4-y}$ [3], the conducting carriers are electron-like. While the crystal structures in both hole- and electron-doped systems have common CuO_2 planes, and both types of oxides exhibit antiferromagnetism (AF) and are insulators at half-band filling, experiments [4, 5] show that the doping dependence of antiferromagnetism in these two systems is very different. In the hole-doped case AF order decreases rapidly with doping, and long-range antiferromagnetic order is destroyed for a doping concentration δ_c of 2–3%. Then, a state with disordered magnetic moments with short-range correlation, possibly a spin-glass-like state, appears. The dependence of AF order on electron doping is much weaker. Doping destroys the AF long-range order only for a doping concentration δ_c of the order of 15%.

These magnetic properties, as well as photoemission results on the superconducting oxides, suggest that electron correlations play an important role. Thus, both the one-band and three-band Hubbard Hamiltonians [6–12] are proposed as model Hamiltonians for the CuO_2 plane of these oxides, where the carriers contributing to superconductivity are mainly located. Although the one-band Hubbard Hamiltonian describes the low-energy excitations equally as well as the three-band Hubbard Hamiltonian, these two Hamiltonians do yield different results for the magnetic properties, particularly on the asymmetrical doping

0953-8984/95/071335+15$19.50

dependence of the magnetic properties between electron and hole doping. Since the degree of freedom for the oxygen orbitals is eliminated from the outset in the one-band Hubbard Hamiltonian, it has perfect symmetry between electron and hole doping. Therefore, we will study the three-band Hubbard Hamiltonian in this paper. Based on the three-band Hubbard Hamiltonian, several calculations (see, for example, [13–16]), were carried out using the Hartree–Fock and Gutzwiller approximations for the hole-doped compounds. All of these studies assume translational symmetry, thus only the magnetically ordered states are included. The critical doping concentration for the transition from the antiferromagnetic to the Pauli paramagnetic state is much larger than the experimentally observed one, $\delta_c \simeq 0.4$ using typical parameters of the Hamiltonian.

It has been shown [17–19] that this discrepancy will disappear if the magnetic moment disorder is included. In fact, the stable hole doping range for the antiferromagnetic phase of hole-doped compounds is drastically reduced once the effect of the magnetic moment disorder is taken into account. By combining the single-site coherent potential approximation and the Hartree–Fock approximation, Yndurain and Martinez [17] have studied the effect of Cu moment disorder on the magnetic phase diagram of hole-doped compounds. They obtained a much smaller δ_c. A similar result was also obtained by Baumgärtel and co-workers [18]. To take into account strong correlations in a more rigorous way, we have also calculated the magnetic phase diagram [19] of the one-band Hubbard Hamiltonian using the slave boson mean field approximation. It is shown that the generalized paramagnetic state with local moments is energetically more favourable than the Pauli paramagnetic state. By using this magnetic phase diagram and adopting a mapping procedure, we are able to obtain a realistic critical hole-doping concentration of a few per cent using reasonable parameters for the three-band Hubbard Hamiltonian [20]. While the paramagnetic state with local moments mimics the spin-glass-like state very well in energy, the underlying physical picture for the destruction of the long-range antiferromagnetism is still unclear. This is because the paramagnetic state with a disordered local magnetic moment is a statistically averaged state. The types of pure states that are mainly responsible for the destruction of the long-range antiferromagnetic state were not analysed.

Therefore, to obtain a better physical understanding of the destruction of the long-range AF state via magnetic textures and domain formation and of the origin of the paramagnetic state with local moments, we have studied the magnetic textures of the three-band Hubbard Hamiltonian with a relaxed symmetrical requirement for the hole-doped high-T_c superconductors [21]. In contrast to the Hartree–Fock calculations made by Verges and co-workers [22, 23] for small clusters with open boundary conditions, we consider a periodic lattice of a supercell consisting of 4×4 cells so that our results may relate to the bulk properties of these superconducting oxides. In our calculation, we use the unrestricted Hartree–Fock approximation and treat the spins as vectors rather than as Ising-like. Our study shows that it is the competition between the antiferromagnetic state and the various magnetic textures that results in the small critical hole-doping concentration for the destruction of the antiferromagnetic state in the hole doped compounds. For the region of parameters studied, the antiferromagnetic state becomes unstable at a hole-doping concentration of 6% with respect to the antiferromagnetic domain-like texture M_7 (see figure 1). This is an important result, as the critical hole-doping concentration could be five times larger if no magnetic textures are introduced. We also conclude from our calculation that the paramagnetic state with a disordered local magnetic moment used in our previous discussion [19, 20] can be viewed as a statistical average over these magnetic textures.

Here we present a comparative study of the magnetic textures using the three-band

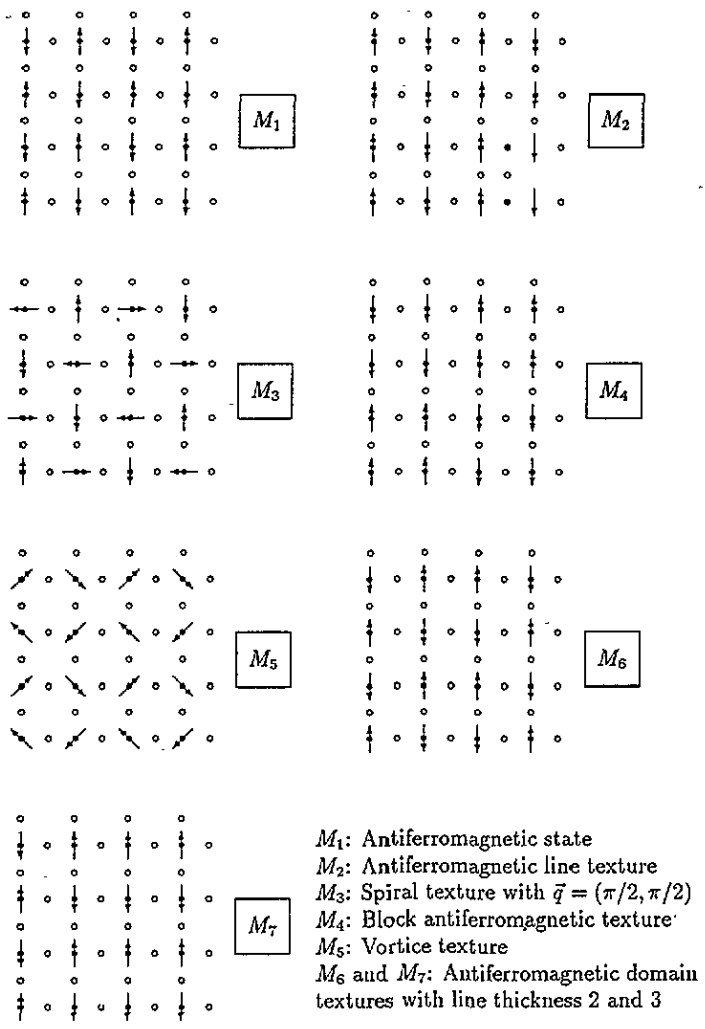

Figure 1. Schematic drawings for the seven types of textures studied in the text. The full dots denote Cu sites, the open dots denote O sites. Only the magnetic moment directions on Cu are indicated (by arrows).

Hubbard Hamiltonian. We analyse the doping dependence of the AF in comparison with other magnetic textures as a function of electron- and hole-doping concentration. Our results show the following. (i) For a hole-doping concentration $\delta > 0.06$, textures consisting of antiferromagnetic domains become more energetically favourable than the long-range antiferromagnetic structure and other textures studied in this paper. Amongst the energetically most favourable domain textures is the one which has larger domain width. This reflects the competition between the kinetic energy (lowered by a ferromagnetically coupled domain wall) and exchange energy (preserved by local antiferromagnetism). (ii) For an electron-doping concentration $-\delta > 0.13$ the spiral texture and domain-like texture become the most favourable. (iii) There is an intrinsic asymmetry between electron-doped and hole-doped high-T_c superconductors: the long-range antiferromagnetic ordering is less rapidly destroyed for electron doping, in agreement with experiment. We find long-range

antiferromagnetic ordering disappears at 6% for the hole-doped system, while it disappears at 13% for the electron-doped system. This suggests that the oxygen orbital degree of freedom is indispensable in an accurate description of the magnetic properties of high-T_c superconductors. Note that a one-band Hubbard Hamiltonian yields an identical doping dependence for electron- and hole-doping due to its symmetry around the half-band filling. Concerning the destruction of the AF state we would like to mention that, among others, Shraiman and Siggia [24] suggested the possibility of a spiral state, while Poilblanc and Rice [25] and Schultz [26] proposed domain-wall states in the one-band Hubbard model.

Our paper is organized as follows. In section 2, we briefly discuss the formalism of the unrestricted Hartree–Fock approximation and the real-space recursion method, which enables us to consider a large supercell in order to study the magnetic textures. The numerical results for the local density of states for various magnetic textures are presented in section 3. Their energies are then compared with the antiferromagnetic phase. In section 4 we present the conclusion.

2. Theory and numerical method

The physical properties of the CuO_2 planes of high-T_c superconducting oxides can be modelled by the three-band Hubbard Hamiltonian [6, 7] written in the hole representation:

$$H = \sum_{is} \epsilon_d d_{is}^+ d_{is} + \sum_{js} \epsilon_p p_{js}^+ p_{js} + \sum_i U d_{i\uparrow}^+ d_{i\uparrow} d_{i\downarrow}^+ d_{i\downarrow} + \sum_{(ij)s} t_{dp}^{ij} (d_{is}^+ p_{js} + \text{HC}) + \sum_{(jj')s} t_{pp}^{jj'} (p_{js}^+ p_{j's} + \text{HC}). \tag{1}$$

Here, d_{is}^+ and p_{js}^+ denote the creation operators of a hole in a Cu-$d_{x^2-y^2}$ state at site i with energy ϵ_d and a hole in an O-$p_{x(y)}$ state at site j with energy ϵ_p, respectively; s refers to the spin. The relevant parameters of the Hamiltonian are t_{dp} for hopping between the copper and oxygen orbitals, t_{pp} for hopping between neighbouring oxygen orbitals, the Hubbard repulsion U, the charge transfer energy $\Delta = (\epsilon_p - \epsilon_d)$, and the doping concentration $\delta = \bar{n}_{CuO_2} - 1$; $\bar{n}_{CuO_2}$ is the average hole number in the CuO_2 cell. For a hole-doped system $\delta > 0$, and for an electron-doped system $\delta < 0$. In the unrestricted Hartree–Fock approximation, the problem amounts to obtaining the solution for the following effective one-particle Hamiltonian [22]:

$$H = \sum_{is} (\epsilon_d + U n_i^d/2) d_{is}^+ d_{is} + \sum_{js} \epsilon_p p_{js}^+ p_{js} - \sum_{i,s,s'} (U/2) m_i^d \cdot d_{is}^+ \sigma_{ss'} d_{is'} + \sum_{(ij)s} t_{dp}^{ij} (d_{is}^+ p_{js} + \text{HC}) + \sum_{(jj')s} t_{pp}^{jj'} (p_{js}^+ p_{j's} + \text{HC}) \tag{2}$$

together with the self-consistent conditions

$$n_i^d = \sum_s \langle d_{is}^+ d_{is} \rangle \tag{3}$$

and

$$m_i^d = \sum_{ss'} \langle d_{is}^+ \sigma_{ss'} d_{is'} \rangle. \tag{4}$$

The self-consistent solutions of this decoupled Hamiltonian give the metastable solutions of the original many-body Hamiltonian. Verges and co-workers [22] found in their small-cluster calculation of the one-band Hubbard Hamiltonian that all the spin textures have planar structures. We will thus also concentrate on the planar magnetic textures of our supercell. By using a different initial configuration for the particle number n_i^d and magnetic moment m_i^d inside the supercell of 4×4 CuO_2 cells, we have studied the convergence of various different magnetic textures. For the supercell as chosen in our calculation, there seems to exist only seven types of stable textures. Other initial configurations turn out to be divergent.

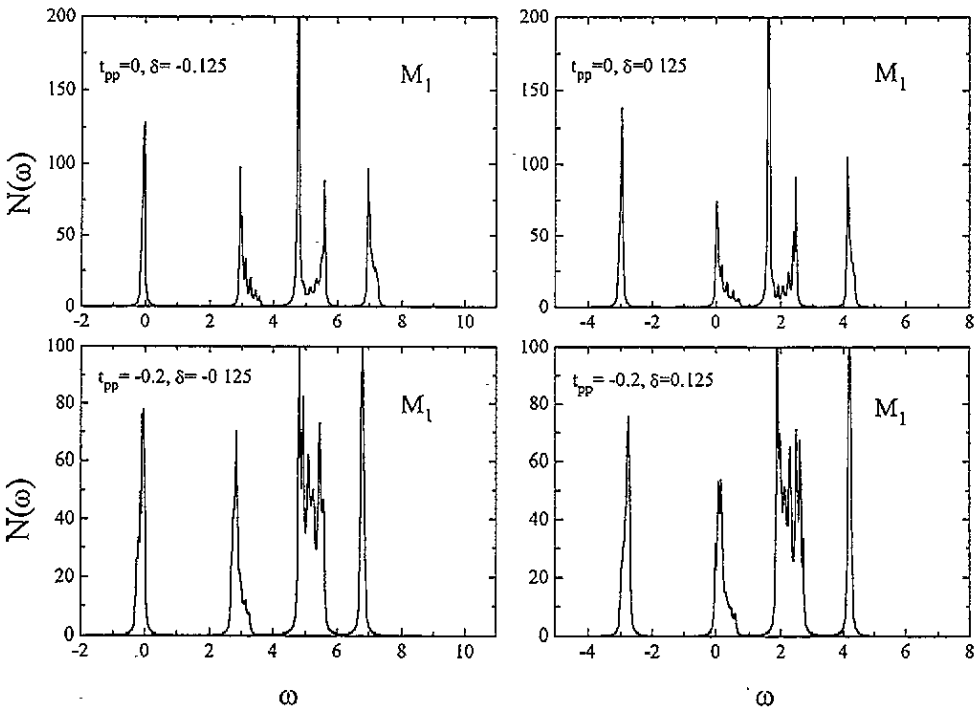

Figure 2. The total densities of states of the supercell $N(\omega) = \sum_{s=1}^{96} -(1/\pi)\mathrm{Im}G(\omega, s)$ for the magnetic texture M_1. The abscissa measures the energy difference with respect to the Fermi energy, $(\omega - E_F)/t_{dp}$, and the ordinate is in units of states per t_{dp}; t_{dp} is the direct hopping between Cu and O sites.

To calculate various physical quantities of the effective one-particle Hamiltonian, such as n_i^d and m_i^d, one needs to determine the local density of states (DOS) for each orbital in the supercell. In our study, a calculation of the local density of states on the different sites of the supercell is implemented using the real space recursion method [27], which provides a systematic way to extend the primitive cell. Instead of diagonalizing the Hamiltonian with the dimension of the number of orbitals in the supercell, the recursion method chooses one particular lattice site, where the local density of states is determined, and tridiagonalizes the Hamiltonian for a certain number of levels; one then writes the Green function as

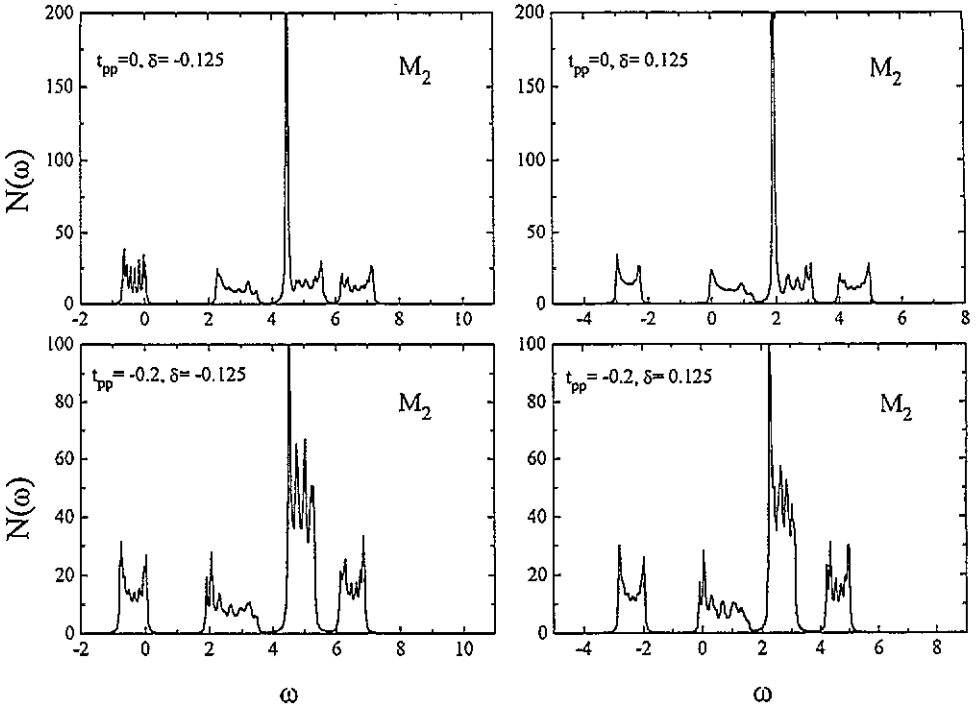

Figure 3. $N(\omega)$ for the magnetic texture M_2.

$$G_{is}(\omega) = \cfrac{b_0^2}{\omega - a_0 - \cfrac{b_1^2}{\omega - a_1 - \cfrac{b_2^2}{\omega - a_2 - \cfrac{b_3^2}{\omega - a_3 - \ldots}}}} . \tag{5}$$

The coefficients a_l and b_i are obtained from the tridiagonalization of the tight-binding Hamiltonian matrix for a given starting orbital. To close the continuous fractional a terminator is required. We have chosen a multiband terminator [28] in our calculation, which can correctly simulate the multiband structure. Note that the number of orbitals involved in the computation is rather large. There are 96 orbitals in the supercell of 4×4 CuO_2 cells (including spin). To extract the transverse spin components, 48 more orbitals with mixed spins have to be calculated. Therefore, the densities of states of 144 orbitals are calculated for each iteration. We have computed 27 levels in this calculation for the continuous fractional coefficients for each orbital in the supercell. This is quite a large number, considering the number of orbitals involved. Note that the total number of iterations required to achieve a convergence depends on the initial trial configuration. In general, the recursion method offers the correct overall features of the density of states; properties depending only on the global quantity of DOS can be reliably obtained. We have also compared our result with an analytic paramagnetic density of states in the special limit $t_{pp} = 0$, and good agreement is achieved.

From the spin-dependent Green function given by (5), one can obtain the corresponding density of states $N_{is}(\omega) = -\mathrm{Im}G_{is}(\omega)/\pi$. The spin-up and spin-down Green functions

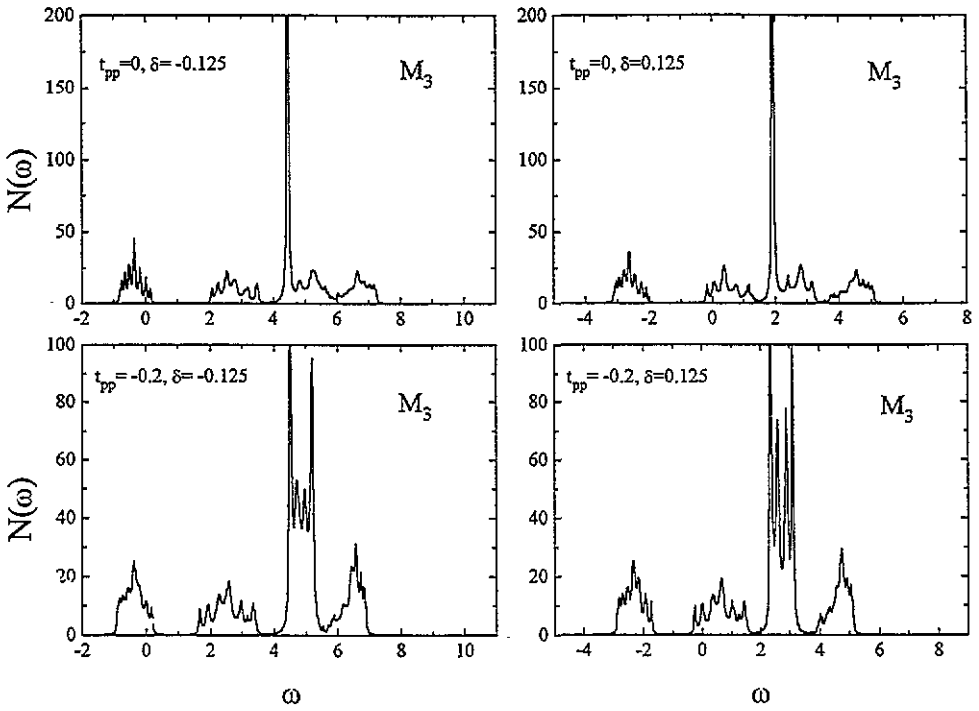

Figure 4. $N(\omega)$ for the magnetic texture M_3.

give the corresponding hole number and z component of the magnetic moment on that site, while the transverse moment component can be extracted from the Green function of the mixed spin-up and spin-down orbital by subtracting the pure spin-up and spin-down components. We will study various magnetic textures and the competition between them for both electron- and hole-doped CuO_2 plane using the unrestricted Hartree–Fock approximation and the recursion method summarized above.

3. Results and discussions

The Fermi surface of the electronic band structure with $t_{pp} = 0$ has a perfect nesting property which favours the antiferromagnetic long-range order. Including the finite O–O hopping matrix enables us to study how the antiferromagnetic long-range order is destroyed as the Fermi surface nesting disappears in the presence of various magnetic textures. Thus, we study the magnetic textures for different O–O hopping matrix elements $t_{pp} = 0$ and -0.2 eV and doping concentrations $\delta = -0.125$, -0.0625, 0, 0.0625 and 0.125. We choose for the Hubbard repulsion $U = 6$ eV, for the on-site energy on oxygen orbital $\epsilon_p = 0$, on the copper orbital $\epsilon_d = -\Delta = -4$ eV and for the direct Cu–O hopping matrix $t_{dp} = 1$ eV.

In the following numerical study, we concentrate on the seven types of magnetic textures shown in figure 1. These include the antiferromagnetic state (M_1), the antiferromagnetic line texture (M_2), spiral texture with wave vector $q = (\pi/2, \pi/2)$ (M_3), block antiferromagnetic texture (M_4), vortex-like texture (M_5), and antiferromagnetic domain-like textures with line thickness 2 (M_6) and 3 (M_7), respectively. Although the number of possible magnetic textures is limited due to the finite size of the supercell, our study already suggests the

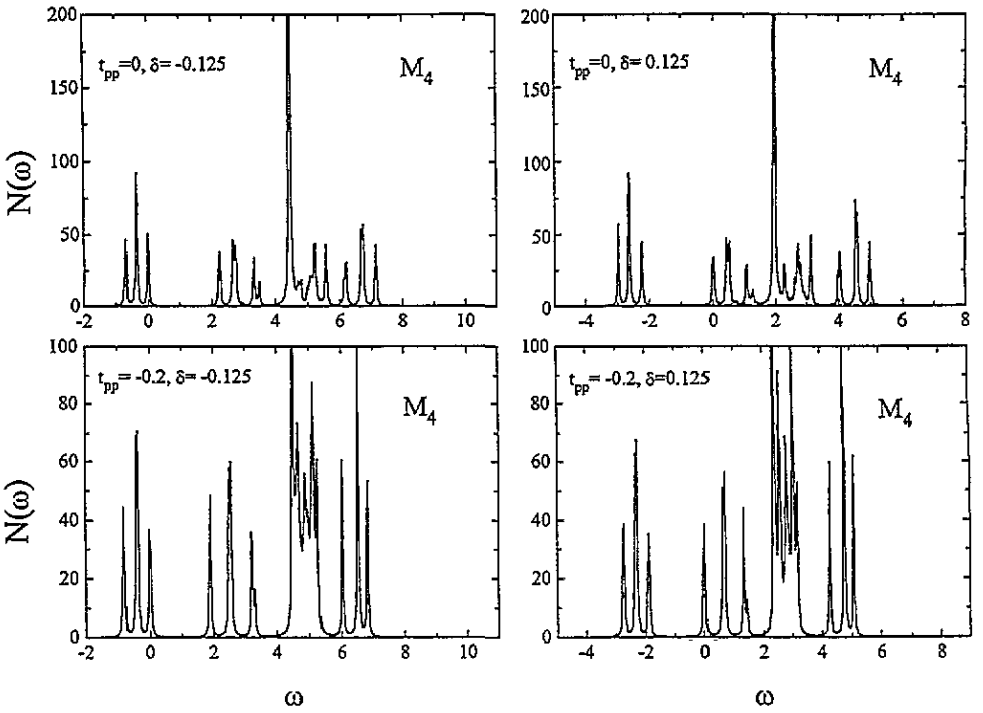

Figure 5. $N(\omega)$ for the magnetic texture M_4.

influence of these textures on the stability of the antiferromagnetic phase. We have also tried some other exotic vortex-like structures, which are found to be the most stable structure in a small cluster with open boundary conditions [22, 23]. However, our self-consistent equation turns out to be non-convergent in those cases. Note that (except the texture M_7) the occupation number and magnitude of the magnetic moment is the same on all Cu sites. The texture M_7 has three different magnetic moments on Cu and O orbitals.

In figures 2–8, we show the total density of states resulting from a sum over the 96 local orbitals of the supercell. Figure 2 shows the total density of states for the antiferromagnetic texture configuration (M_1) for both electron and hole doping and for different O–O hopping matrix t_{pp}. In the case of $t_{pp} = 0$, there is a δ-function-like peak near the middle of the spectra due to the decoupled oxygen orbital. The other oxygen orbital together with copper orbital form bonding and antibonding orbitals below and above this δ-function-like peak. Both of these bands split under the influence of the antiferromagnetic long-range order. As can be seen from the figure, the direct nearest-neighbour oxygen–oxygen hopping couples the originally decoupled oxygen orbital with the other orbitals. The antiferromagnetic gap also decreases because of the t_{pp} hopping. The effect of doping on the density of states is to shift the Fermi energy upward into the conduction band for the hole-doped system and downward into the valence band for the electron-doped system.

The density of states of the antiferromagnetic line texture (M_2) is shown in figure 3. It can be understood as reflecting the following two physical processes. The ferromagnetic ordering along the y direction causes the one-dimensional-like density of states with the singularity at the edges of the bands, and antiferromagnetic ordering along the x axis causes the band splitting. As before, only one oxygen orbital couples to the copper orbital when

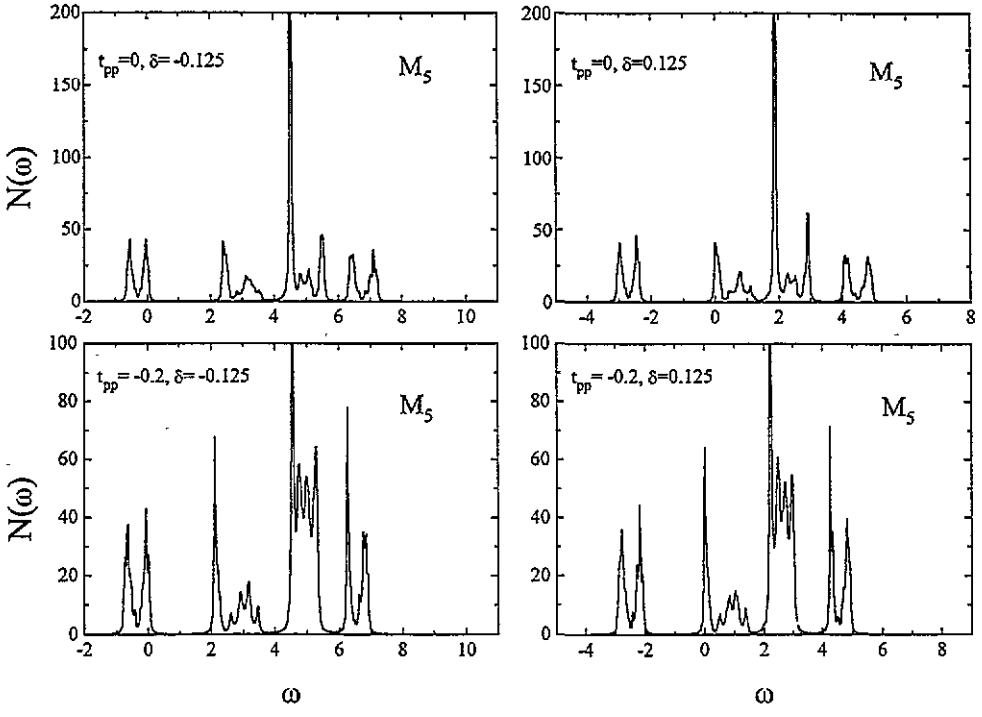

Figure 6. $N(\omega)$ for the magnetic texture M_5.

$t_{pp} = 0$. The decoupled oxygen orbital merges with the antibonding band when t_{pp} is switched on. Note that the bandwidth in this case is twice as large as the antiferromagnetic bandwidth. Hence, the holes move more easily than in the antiferromagnetic phase. The effect of doping is the same as in figure 2.

In figure 4 we illustrate the density of states for the spiral texture (M_3) which has a wavevector $q = (\pi/2, \pi/2)$. Due to the periodic boundary condition, this is the only possible spiral texture in our chosen supercell. The bandwidth for the conduction and valence bands is similar to that of the antiferromagnetic line texture (M_2). The major peak positions are almost the same as in the case of the antiferromagnetic texture (M_1). Due to the wider bands, the insulator gap is 30% smaller than the antiferromagnetic one. The effects of the direct O–O hopping matrix t_{pp} and doping process are the same as in figure 3, except that the maximum DOS occurs in the centre of split bands.

As shown in figure 5, in the case of the block antiferromagnetic texture (M_4), there is a further band splitting due to the block structure and every subband splits into three. One sees from these figures that rich structure in the density of states appears when more complicated magnetic textures are considered. This is to be expected since the primitive cell contains more orbitals, which compose the subbands in the spectra.

Figure 6 shows the total density of states for the vortex-like magnetic texture (M_5). As can easily be seen, the density of states resembles that of the antiferromagnetic line texture, although there is a complete band splitting in this case. One recognizes that the net magnetization of the y layer alternates along the x axis, in spite of the fact that the Cu spins do not orientate along the y axis. This makes the density of states in figures 3 and 6 similar.

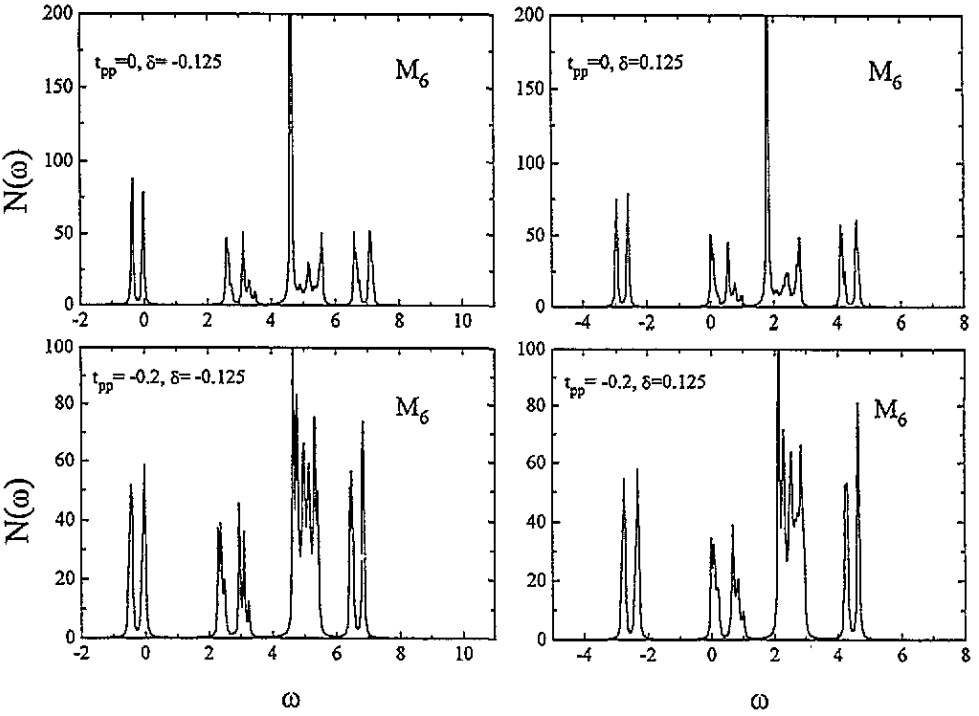

Figure 7. $N(\omega)$ for the magnetic texture M_6.

The densities of states for the last two magnetic textures (M_6 and M_7) are shown in figures 7 and 8. Figure 7 looks very similar to figure 6, while figure 8 is similar to figure 5, except for a smaller bandwidth. Note that the little nipple found in some of the density of states may be due to the limited number of levels used in the recursion routine. As mentioned in the introduction, the recursion method generally offers good overall features of the DOS. This ensures that quantities such as local magnetic moments and energy can be calculated reliably, since they involve an integration over the density of states.

To understand the influence of these magnetic textures on the destruction of antiferromagnetism for both electron and hole doping, we also compared the energies of these various textures. They are summarized in table 1 and 2 for $t_{pp} = 0$ and $t_{pp} = -0.2\,\text{eV}$, respectively. The first column lists the seven magnetic textures as shown in figure 1. The term δ denotes the average hole-doping concentration for one CuO_2 cell, with $\delta > 0$ for hole doping and $\delta < 0$ for electron doping; E_F and E_B are the Fermi energy and the energy of the supercell, while m_x^d, m_y^d, m_x^p, m_y^p represent the Cu and O moment components in the x and y directions, respectively. Note that only moments with different magnitudes are listed, and zero oxygen moments in the textures M_2, M_4, M_6 are not included in the tables. Comparing E_B of various magnetic textures for half-filled bands, one concludes that the antiferromagnetic phase has the lowest energy. Therefore it is the stable state, in agreement with experimental observation [4, 5]. In table 1, the smallest energy difference between the antiferromagnetic phase and other textures is 0.08 eV. However, with doping, one notices that the antiferromagnetic phase becomes unstable with respect to the magnetic textures M_6 and M_7 at a hole doping concentration $\delta = 0.0625$, and unstable to the magnetic textures M_3 and M_4 at an electron doping concentration $\delta = -0.125$. The most stable textures at these

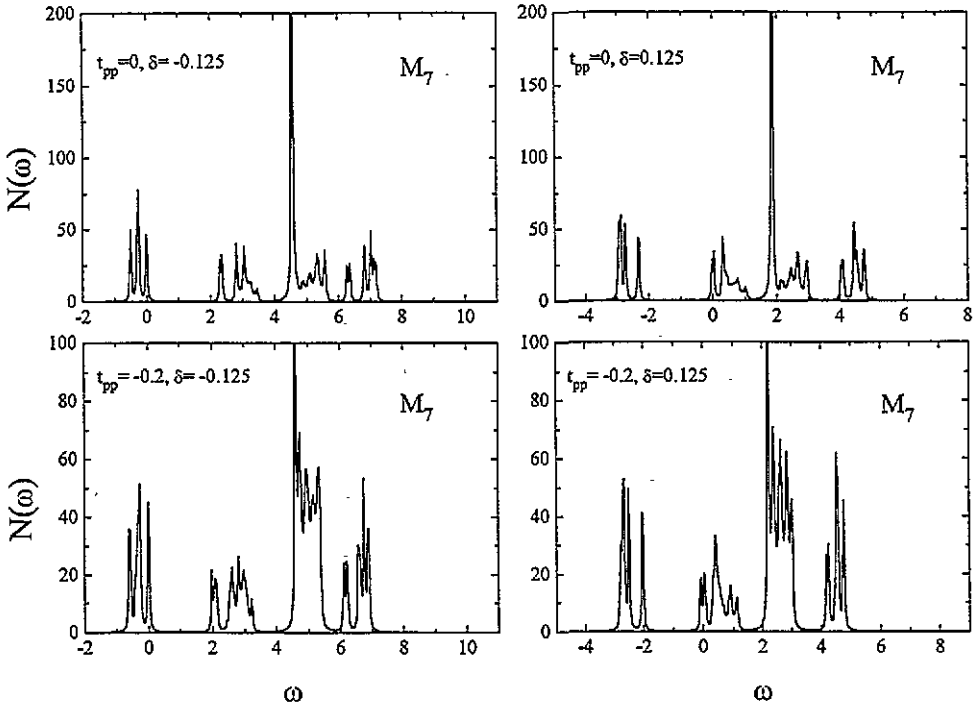

Figure 8. $N(\omega)$ for the magnetic texture M_7.

dopings are the large domain-like texture M_7 for hole-doped system and the spiral texture M_3 for the electron-doped system. Our study shows that these magnetic textures have a much lower energy than a Pauli paramagnet; it is the competition between the antiferromagnetic state and various magnetic textures that results in the small critical doping concentration for both the hole- and electron-doped systems. Our result may also indicate that a spin-glass-like phase occurs after the destruction of the antiferromagnetic phase for both hole- and electron-doped oxides (since the existence of finite magnetic moments is a prerequisite of the spin-glass phase).

For $t_{pp} = -0.2\,\text{eV}$, one finds from table 2 that the magnetic moments on Cu sites are reduced, while the oxygen magnetic moments that exist in some of the textures increase. This means that t_{pp} favours a more uniform distribution of moments amongst Cu and O sites. Since t_{pp} enhances the hole mobility in the CuO_2 plane, the total energy decreases for all the magnetic textures. While the antiferromagnetic state has the lowest energy at half-band filling, the energy difference between this state and other magnetic textures decreases rapidly and the AF state becomes unstable against the large domain-like texture M_7 for a hole-doping concentration $\delta = 0.0625$ and for and electron-doping concentration $\delta = -0.125$. Therefore, the mechanism for the destruction of the antiferromagnetism as a function of doping also holds for finite t_{pp}. Our study also shows that there is an intrinsic asymmetry between electron- and hole-doped superconducting oxides; the antiferromagnetic state is less rapidly destroyed in electron-doped than in hole-doped systems, in agreement with experiment [4, 5]. Note that the low-energy states in our case are the domain-like textures for hole doping and spiral- and domain-like textures for electron doping, and not the vortex-like texture in the finite-cluster calculations with open boundary conditions [22, 23]. Thus, our result agrees

Table 1. Fermi energy E_F, total energy of the supercell E_B, and magnetic moment projections in the x and y directions on the Cu site (m_x^d, m_y^d) and on the O site (m_x^p, m_y^p) for various magnetic textures M_i as a function of doping concentration δ with the O–O hopping $t_{pp} = 0$.

Texture	δ	$-E_F$	$-E_B$	m_x^d	m_y^d	m_x^p	m_y^p
M_1	−0.1250	4.765	68.389	0.000	0.722	0.000	0.000
	−0.0625	4.719	73.142	0.000	0.778	0.000	0.000
	0.0000	3.086	77.603	0.000	0.829	0.000	0.000
	0.0625	1.622	79.469	0.000	0.801	0.000	0.000
	0.1250	1.607	81.092	0.000	0.766	0.000	0.000
M_2	−0.1250	4.479	68.477	0.000	0.732	0.000	0.064
	−0.0625	4.443	72.932	0.000	0.788	0.000	0.065
	0.0000	3.334	77.243	0.000	0.842	0.000	0.066
	0.0625	1.955	79.362	0.000	0.816	0.000	0.044
	0.1250	1.927	81.355	0.000	0.781	0.000	0.026
M_3	−0.1250	4.443	68.590	0.000	0.729	0.034	0.034
	−0.0625	4.360	73.008	0.000	0.789	0.033	0.033
	0.0000	3.288	77.234	0.000	0.842	0.033	0.033
	0.0625	2.057	79.446	0.000	0.811	0.023	0.023
	0.1250	1.925	81.443	0.000	0.781	0.012	0.012
M_4	−0.1250	4.451	68.552	0.000	0.731	0.000	0.065
	−0.0625	4.422	72.939	0.000	0.788	0.000	0.065
	0.0000	3.223	77.211	0.000	0.842	0.000	0.065
	0.0625	1.974	79.323	0.000	0.813	0.000	0.045
	0.1250	1.958	81.478	0.000	0.783	0.000	0.025
M_5	−0.1250	4.520	68.429	0.517	0.517	0.045	0.000
	−0.0625	4.477	72.922	0.556	0.556	0.046	0.000
	0.0000	3.379	77.254	0.595	0.595	0.047	0.000
	0.0625	1.895	79.350	0.574	0.574	0.032	0.000
	0.1250	1.872	81.233	0.555	0.555	0.015	0.000
M_6	−0.1250	4.616	68.441	0.000	0.726	0.000	0.064
	−0.0625	4.589	73.051	0.000	0.781	0.000	0.064
	0.0000	3.881	77.523	0.000	0.835	0.000	0.065
	0.0625	1.799	79.514	0.000	0.809	0.000	0.042
	0.1250	1.790	81.274	0.000	0.775	0.000	0.015
M_7	−0.1250	4.557	68.495	0.000	0.726	0.000	−0.005
	——	——	——	0.000	−0.811	0.000	0.063
	——	——	——	0.000	0.645	0.000	−0.005
	−0.0625	4.532	73.055	0.000	0.783	0.000	−0.002
	——	——	——	0.000	−0.813	0.000	0.064
	——	——	——	0.000	0.753	0.000	−0.002
	0.0000	3.041	77.383	0.000	0.835	0.000	0.001
	——	——	——	0.000	−0.827	0.000	0.064
	——	——	——	0.000	0.842	0.000	0.000
	0.0625	1.865	79.557	0.000	0.810	0.000	−0.002
	——	——	——	0.000	−0.825	0.000	0.036
	——	——	——	0.000	0.792	0.000	0.000
	0.1250	1.854	81.425	0.000	0.777	0.000	−0.005
	——	——	——	0.000	−0.823	0.000	0.003
	——	——	——	0.000	0.722	0.000	0.000

Table 2. Same notation as in table I, but with $t_{pp} = -0.2$.

Texture	δ	$-E_F$	$-E_B$	m_x^d	m_y^d	m_x^p	m_y^p
M_1	−0.1250	4.788	69.494	0.000	0.693	0.000	0.000
	−0.0625	4.759	74.328	0.000	0.750	0.000	0.000
	0.0000	3.520	78.845	0.000	0.780	0.000	0.000
	0.0625	1.881	80.940	0.000	0.773	0.000	0.000
	0.1250	1.861	82.798	0.000	0.741	0.000	0.000
M_2	−0.1250	4.483	69.534	0.000	0.710	0.000	0.071
	−0.0625	4.446	73.978	0.000	0.767	0.000	0.072
	0.0000	3.415	78.274	0.000	0.820	0.000	0.072
	0.0625	2.321	80.732	0.000	0.794	0.000	0.051
	0.1250	2.247	82.959	0.000	0.765	0.000	0.028
M_3	−0.1250	4.463	69.573	0.000	0.708	0.036	0.036
	−0.0625	4.357	74.024	0.000	0.766	0.036	0.036
	0.0000	3.306	78.254	0.000	0.821	0.036	0.036
	0.0625	2.243	80.835	0.000	0.794	0.024	0.024
	0.1250	2.314	83.221	0.000	0.759	0.013	0.013
M_4	−0.1250	4.464	69.555	0.000	0.707	0.000	0.072
	−0.0625	4.434	74.029	0.000	0.766	0.000	0.072
	0.0000	3.869	78.381	0.000	0.820	0.000	0.073
	0.0625	2.358	80.761	0.000	0.793	0.000	0.049
	0.1250	2.337	83.078	0.000	0.763	0.000	0.023
M_5	−0.1250	4.516	69.378	0.497	0.497	0.050	0.000
	−0.0625	4.486	73.967	0.540	0.540	0.050	0.000
	0.0000	3.248	78.236	0.576	0.576	0.051	0.000
	0.0625	2.194	80.608	0.558	0.558	0.036	0.000
	0.1250	2.175	82.816	0.530	0.530	0.021	0.000
M_6	−0.1250	4.629	69.480	0.000	0.701	0.000	0.070
	−0.0625	4.603	74.094	0.000	0.758	0.000	0.070
	0.0000	3.262	78.503	0.000	0.809	0.000	0.070
	0.0625	2.116	80.827	0.000	0.783	0.000	0.046
	0.1250	2.105	82.921	0.000	0.749	0.000	0.015
M_7	−0.1250	4.573	69.582	0.000	0.701	0.000	−0.005
	——	——	——	0.000	−0.781	0.000	0.070
	——	——	——	0.000	0.620	0.000	−0.005
	−0.0625	4.550	74.146	0.000	0.757	0.000	−0.001
	——	——	——	0.000	−0.785	0.000	0.071
	——	——	——	0.000	0.730	0.000	−0.001
	0.0000	3.451	78.562	0.000	0.809	0.000	0.001
	——	——	——	0.000	−0.800	0.000	0.073
	——	——	——	0.000	0.821	0.000	0.000
	0.0625	2.212	80.939	0.000	0.787	0.000	−0.001
	——	——	——	0.000	−0.798	0.000	0.040
	——	——	——	0.000	0.770	0.000	0.000
	0.1250	2.163	83.004	0.000	0.755	0.000	−0.005
	——	——	——	0.000	−0.797	0.000	0.003
	——	——	——	0.000	0.691	0.000	0.000

with the studies by Poilblanc and Rice [25] and Schultz [26] that domain wall states replace the AF state at a finite doping concentration. As mentioned earlier, our calculation is made

on a 4×4 CuO_2 supercell with periodic boundary conditions. Enlarging the supercell size will allow more possible magnetic textures; this will lower the energy bound of magnetic textures with respect to the AF state and slightly reduce the critical doping concentration for the destruction of the AF state. However, from our studies using other methods [19, 20], we believe that the main conclusions concerning the asymmetry between electron and hole dopings as well as the critical doping concentration for the destruction of the AF state will remain valid and independent of the supercell size. It is of interest to note that the phase space where superconductivity occurs indicates that spin correlations may play an important role.

4. Conclusion

In conclusion, we have studied various magnetic textures in the three-band Hubbard Hamiltonian. We find that the magnetic textures with finite magnetic moments have a much lower energy as compared with the Pauli paramagnetic state. Our results show that domain-like textures have the lowest energy for a finite hole-doping concentration, and spiral- and domain-like textures have the lowest energy for a finite electron-doping concentration. We find, in agreement with experimental observation, that the state resulting after the destruction of the antiferromagnetic phase has a finite magnetic moment. In particular, we show that the doping effect is intrinsically asymmetrical for the electron- and hole-doped high-T_c superconductors and the antiferromagnetic state is less rapidly destroyed in electron-doped compounds than in hole-doped compounds. Our study also implies that the result obtained for a small cluster with open boundary conditions may not yield the bulk physical properties. Our result clearly demonstrates the difference between the three-band Hubbard Hamiltonian and the one-band Hubbard Hamiltonian, since the latter has perfect symmetry between electron and hole doping.

In summary, we find that (i) for a hole-doping concentration $\delta > 0.06$ textures consisting of antiferromagnetic domains become the most favourable state; (ii) for an electron-doping concentration $-\delta > 0.13$ the spiral texture and domain-like texture become the most favourable states depending on the value of the direct O–O hopping t_{pp}; (iii) there is an intrinsic asymmetry of the magnetic properties of the three-band Hubbard Hamiltonian between electron doping and hole doping, in agreement with experimental observations of high-T_c superconductors [4, 5]. Our result suggests that the degree of freedom of the oxygen orbitals is indispensable for an accurate description of the magnetic properties of high-T_c superconductors.

Acknowledgments

This work has been supported in part by the Education Commission of China (WZ) and by the Bundesministerium für Forschung und Technologie (KHB).

References

[1] Bednorz J G and Müller K A 1986 *Z. Phys.* B **64** 189
[2] Wu M K, Ashburn J R, Torng C J, Hor P H, Meng R L, Gao L, Huang Z J, Wang Y Q and Chu C W 1987 *Phys. Rev. Lett.* **58** 908
[3] Tokura Y, Takagi H and Uchida S 1989 *Nature* **337** 345

Takagi H, Uchida S and Tokura Y 1989 *Phys. Rev. Lett.* **62** 1197
[4] Thurston T R, Matsuda M, Kakurai K, Yamada K, Endoh Y, Birgeneau R J, Gehring P M, Hidaka Y, Kastner M A, Murakami T and Shirane G 1990 *Phys. Rev. Lett.* **65** 263
[5] Luke G M, Le L P, Sternlieb B J, Uemura Y J, Brewer J H, Kadono R, Kiefl R F, Kreitzman S R, Riseman T M, Stronach C E, Davis M R, Uchida S, Takagi H, Tokura Y, Hidaka Y, Murakami T, Gopalakrishman J, Sleight A W, Subramanian M A, Early E A, Markert J T, Maple M B and Seaman C L 1990 *Phys. Rev.* B **42** 7981
[6] Emery V J 1987 *Phys. Rev. Lett.* **58** 2794
[7] Varma C M, Schmitt-Rink S and Abrahams E 1987 *Solid State Commun.* **62** 681
[8] Anderson P W 1987 *Science* **235** 1196
Anderson P W, Baskaran G, Zou Z and Hsu T 1987 *Phys. Rev. Lett.* **58** 2790
[9] Ruckenstein A E, Hirschfeld P and Appel J 1988 *Phys. Rev.* B **36** 857
[10] Lee P A and Read N 1987 *Phys. Rev. Lett.* **58** 2691
[11] Hirsch J E 1987 *Phys. Rev. Lett.* **59** 228
[12] Schrieffer J R, Wen X-G and Zhang S-C 1988 *Phys. Rev. Lett.* **60** 944; 1989 *Phys. Rev.* B **39** 11663
[13] Balseiro C A, Avignon M, Rojo A G and Alascio B 1989 *Phys. Rev. Lett.* **62** 2624
[14] Oleś A M and Zaanen J 1989 *Phys. Rev.* B **39** 9175
[15] Peter D, Mayou D and Cyrot M 1989 *J. Physique* C **162–4** 199
[16] Weiyi Zhang, Avignon M and Bennemann K H 1990 *Phys. Rev.* B **42** 10192; 1991 *Phys. Rev.* B **43** 11426
[17] Yndurain F and Martinez G 1991 *Phys. Rev.* B **43** 3691
[18] Baumgärtel G, Schmalian J and Bennemann K H 1993 *Phys. Rev.* B **48** 3983
[19] Weiyi Zhang, Avignon M and Bennemann K H 1992 *Phys. Rev.* B **45** 12478
[20] Weiyi Zhang and Bennemann K H 1992 *Phys. Rev.* B **45** 12487
[21] Weiyi Zhang and Bennemann K H 1993 *Phys. Rev.* B **47** 8030
[22] Vergés J A, Louis E, Lomdahl P S, Guinea F and Bishop A R 1991 *Phys. Rev.* B **43** 6099
[23] Louis E, Guinea F and Vergés J A 1991 *Phys. Scri.* **T39** 140
[24] Shraiman B I and Siggia E D 1988 *Phys. Rev. Lett.* **61** 467
[25] Poilblanc D and Rice T M 1989 *Phys. Rev.* B **39** 9749
[26] Schultz H J 1990 *Phys. Rev. Lett.* **64** 1445
[27] Heine V, Haydock R and Kelly M J 1980 *Solid State Phys.* **35** 215
[28] Haydock R and Nex C M M 1984 *J. Physique* C **17** 4783